



HAL
open science

Ozone production from the 2004 North American boreal fires

G.C. Pfister, L.K. Emmons, P.G. Hess, R. Honrast, J.F. Lamarque, M. Val Martin, R.C. Owen, M.A. Avery, E.V. Browell, J.S. Holloway, et al.

► **To cite this version:**

G.C. Pfister, L.K. Emmons, P.G. Hess, R. Honrast, J.F. Lamarque, et al.. Ozone production from the 2004 North American boreal fires. *Journal of Geophysical Research: Atmospheres*, 2006, 111, pp.D24S07. 10.1029/2006JD007695 . hal-00563718

HAL Id: hal-00563718

<https://hal.science/hal-00563718>

Submitted on 25 Jun 2022

HAL is a multi-disciplinary open access archive for the deposit and dissemination of scientific research documents, whether they are published or not. The documents may come from teaching and research institutions in France or abroad, or from public or private research centers.

L'archive ouverte pluridisciplinaire **HAL**, est destinée au dépôt et à la diffusion de documents scientifiques de niveau recherche, publiés ou non, émanant des établissements d'enseignement et de recherche français ou étrangers, des laboratoires publics ou privés.

Copyright

Ozone production from the 2004 North American boreal fires

G. G. Pfister,¹ L. K. Emmons,¹ P. G. Hess,¹ R. Honrath,² J.-F. Lamarque,¹ M. Val Martin,² R. C. Owen,² M. A. Avery,³ E. V. Browell,³ J. S. Holloway,⁴ P. Nedelec,⁵ R. Purvis,⁶ T. B. Ryerson,⁴ G. W. Sachse,³ and H. Schlager⁷

Received 23 June 2006; revised 13 September 2006; accepted 13 October 2006; published 16 December 2006.

[1] We examine the ozone production from boreal forest fires based on a case study of wildfires in Alaska and Canada in summer 2004. The model simulations were performed with the chemistry transport model, MOZART-4, and were evaluated by comparison with a comprehensive set of aircraft measurements. In the analysis we use measurements and model simulations of carbon monoxide (CO) and ozone (O₃) at the PICO-NARE station located in the Azores within the pathway of North American outflow. The modeled mixing ratios were used to test the robustness of the enhancement ratio $\Delta O_3/\Delta CO$ (defined as the excess O₃ mixing ratio normalized by the increase in CO) and the feasibility for using this ratio in estimating the O₃ production from the wildfires. Modeled and observed enhancement ratios are about 0.25 ppbv/ppbv which is in the range of values found in the literature and results in a global net O₃ production of 12.9 ± 2 Tg O₃ during summer 2004. This matches the net O₃ production calculated in the model for a region extending from Alaska to the east Atlantic (9–11 Tg O₃) indicating that observations at PICO-NARE representing photochemically well aged plumes provide a good measure of the O₃ production of North American boreal fires. However, net chemical loss of fire-related O₃ dominates in regions far downwind from the fires (e.g., Europe and Asia) resulting in a global net O₃ production of 6 Tg O₃ during the same time period. On average, the fires increased the O₃ burden (surface –300 mbar) over Alaska and Canada during summer 2004 by about 7–9% and over Europe by about 2–3%.

Citation: Pfister, G. G., et al. (2006), Ozone production from the 2004 North American boreal fires, *J. Geophys. Res.*, *111*, D24S07, doi:10.1029/2006JD007695.

1. Introduction

[2] Ozone (O₃) plays a central role in tropospheric chemistry as a primary source of hydroxyl radicals and, by being toxic in nature, has negative impacts on human and plant health. It is also estimated to be the third most important anthropogenic greenhouse gas [Ramswamy *et al.*, 2001]. Anthropogenic sources and biomass burning release O₃ precursors including carbon monoxide (CO), nitrogen oxides (NO_x) and volatile organic compounds (VOCs) into the atmosphere. Photochemical reaction of CO and VOCs with the hydroxyl radical in the presence of NO_x and sunlight results in the production of O₃.

[3] The production of tropospheric ozone in the Northern midlatitudes is largely impacted by anthropogenic sources

[Chameides and Tan, 1981; Levy *et al.*, 1985]. Significant ozone enhancements have been observed in individual plumes of boreal forest fires [Wofsy *et al.*, 1992; Goode *et al.*, 2000; Forster *et al.*, 2001; McKeen *et al.*, 2002; Jaffe *et al.*, 2004; Honrath *et al.*, 2004; Lapina *et al.*, 2006], and measurements in combination with chemical transport simulations have been used in various studies to estimate the amount of ozone produced from boreal fires [Mauzerall *et al.*, 1996; McKeen *et al.*, 2002]. However, the large-scale impacts of high-latitude biomass burning on the hemispheric tropospheric ozone budget are poorly quantified.

[4] Here we apply a chemical transport model to evaluate various techniques used for estimating the ozone production from a specific source, and include various model tracers to gain a detailed insight into the limitations of these methods. We combine model analysis with observations of CO and O₃ to quantify contributions of boreal fires to Northern Hemispheric CO and O₃ burdens, a topic not very well explored so far. Our analysis focuses on fires in Alaska and Canada in summer 2004. These fires were the largest on record for Alaska, and the CO emissions for the North American boreal region has been estimated as 30 ± 5 Tg for June through August [Pfister *et al.*, 2005]. A total of about 11 million acres were burned in Alaska and Canada during that time period. The study is supported by a comprehensive set of observations collected during the International Consortium for At-

¹National Center for Atmospheric Research, Boulder, Colorado, USA.

²Department of Civil and Environmental Engineering, Michigan Technological University, Houghton, Michigan, USA.

³NASA Langley Research Center, Hampton, Virginia, USA.

⁴National Oceanic and Atmospheric Administration, Boulder, Colorado, USA.

⁵Centre National de la Recherche Scientifique, Toulouse, France.

⁶Facility for Airborne Atmospheric Measurement, Cranfield, UK.

⁷German Aerospace Center, Oberpfaffenhofen, Germany.

ospheric Research on Transport and Transformation (ICARTT) campaign.

[5] CO is a long-lived tracer, and the relationship between mixing ratios of O₃ and CO in transported regional plumes can be used as an indicator for the magnitude of net O₃ production from selected sources [Parrish *et al.*, 1993]. It has been found that the enhancement ratio ($\Delta\text{O}_3/\Delta\text{CO}$), given as the excess O₃ mixing ratio normalized by the increase in CO concentrations, is typically smaller for boreal forest fires than for tropical biomass and savannah burning or urban and industrial plumes, because of a lower NO_x:CO emission ratio in boreal forest fires compared to the other sources [e.g., Andreae *et al.*, 1994; Wofsy *et al.*, 1992]. $\Delta\text{O}_3/\Delta\text{CO}$ of fire plumes is also expected to change with plume age. For example, Yokelson *et al.* [2003] found an increase from 0.09 ppbv/ppbv in fresh tropical biomass-burning plumes to 0.22 ppbv/ppbv for plumes 2–4 days old. Thus O₃ production downwind from the source region must be accounted for.

[6] The structure of this paper is the following. After the Introduction we discuss the model simulations and model evaluation in sections 2 and 3, respectively. In section 4 we describe CO and O₃ in situ measurements taken at the PICO-NARE station located in the Azores. These observations were used in combination with model simulations to investigate the O₃ production from the fires in Alaska and Canada in summer 2004. Section 5 discusses and evaluates different techniques for calculating the enhancement ratio and analyzes the O₃ production due to emissions from the fires. The analysis is supported by incorporating fire tracers for CO and O₃ into the model and by performing model simulations with and without fire emissions. Finally, we investigate the contributions these fires had on the Northern Hemispheric and regional budgets of CO and O₃. Section 6 summarizes our findings.

2. Model Simulation

[7] The model for ozone and related chemical tracers (MOZART) chemistry transport model has been developed at the National Center for Atmospheric Research, the Geophysical Fluid Dynamics Laboratory and the Max-Planck Institute for Meteorology. In this study we are using version 4 (L. K. Emmons *et al.*, Sensitivity of chemical budgets to meteorology in MOZART-4, manuscript in preparation, 2006). Modifications from version 2 published in Horowitz *et al.* [2003] include, amongst others, a more complete description of anthropogenic hydrocarbon chemistry, the inclusion of tropospheric aerosols (extended from the work of Tie *et al.* [2001, 2005]), and online calculations of dry deposition, H₂O, and biogenic emissions.

[8] We run the model at a horizontal resolution of $\sim 2.8^\circ$ by 2.8° . The meteorological fields for 2004 for driving MOZART were taken from the National Centers for Environmental Prediction (NCEP) National Center for Atmospheric Research Re-Analysis [Kistler *et al.*, 2001] and were interpolated from a 6-hour time resolution to the 20-min time steps of the simulations. The vertical resolution of the meteorological fields and hence the model consists of 28 hybrid levels ranging from the surface up to 2 hPa.

[9] Biofuel and fossil fuel emissions used in this study were taken from the European Union project POET (Precursors of Ozone and their Effects in the Troposphere) [Granier *et al.*, 2005]. Over the continental US, the anthropogenic emissions are based on the U.S. EPA NEI-99 inventory (National Emissions Inventory, base year 1999, version 3) (*EPA Clearinghouse for Inventories and Emissions Factors: 1999 National Emission Inventory Documentation and Data, Final Version 3.0*, available at <http://www.epa.gov/ttn/chief/net/1999inventory.html>). For the Alaska and Canada region, the biomass-burning emissions for CO for 2004 were taken from an inverse modeling study [Pfister *et al.*, 2005], and emissions for NO_x and VOCs were deduced from this inventory by applying emission factors based on Andreae and Merlet [2001]. At the time these simulations were run, an emissions inventory for the year 2004 for biomass-burning sources outside North America was not available. A comparison of CO data from the Measurements Of Pollution In The Troposphere (MOPITT) remote sensing instrument for 2000–2004 showed that the global biomass-burning activity in summer 2004 was similar to 2002 and for this reason we used a 2002 biomass-burning inventory based on ATSR fire counts [Granier *et al.*, 2005].

[10] Our model simulations cover the months from June through August 2004 with a spin-up phase beginning in August 2003. We performed three different simulations. Two of these include emissions from the Alaskan and Canadian wildfires, and are abbreviated as BB in the following. In one of these simulations (BBsrf), the wildfire emissions were released at the lowest model layer and distributed in the boundary layer by the model boundary layer scheme. Studies [Fromm *et al.*, 2005; Damoah *et al.*, 2006] have shown that that fire induced convective clouds might transport fire emissions rapidly to higher altitude. To test the sensitivity of our model to the emissions injection height, we performed another simulation (BBvert), where the emissions were distributed evenly with regard to number density between the surface and 9 km altitude. The 9 km altitude represents an upper limit for the injection height based on estimates derived from the Multi-Angle Imaging Spectro-Radiometer (MISR) and the Moderate Resolution Imaging Spectro-Radiometer (MODIS) [Averill *et al.*, 2005]. In a third simulation (noBB) used as a reference, the emissions of the wildfires in Alaska and Canada were set to zero.

[11] We included two fire tracers in the model. Tracers are emitted or produced from a specific source, but undergo the same transport, chemistry, and physical processes as the standard species. The first tracer incorporated into the simulations is a CO fire tracer (CO_f), i.e., CO released from the Alaska/Canada wildfires. For the second tracer we tagged the O₃ production resulting from hydrocarbon or CO oxidation in association with the emissions of NO_x from the fires. We refer to this tracer as O₃^{NO_x} in the following. The tagging technique for O₃^{NO_x} takes into account the recycling of NO_x from reservoirs such as PAN by applying tags to all nitrogen-containing species. Although there are some minor pathways to create O₃ without the presence of NO_x, the accuracy of the tagging technique has been estimated as better than 95% on a monthly basis [Lamarque *et al.*, 2005]. The statistical

Table 1. List of Aircraft Measurements Included in the Evaluation of the Model Simulations^a

Aircraft	Species	Instrument	Reference
NASA-DC8	CO	Tunable diode laser absorption	<i>Sachse et al.</i> [1987]
	O ₃	NO chemiluminescence	M. A. Avery et al. (submitted manuscript, 2006) ^b
	O ₃	airborne differential absorption lidar (DIAL)	<i>Browell et al.</i> [2003]
NOAA-P3	CO	VUV CO fluorescence	<i>Holloway et al.</i> [2000]
	O ₃	NO chemiluminescence	<i>Ryerson et al.</i> [1998]
UK BAE146	CO	VUV resonance fluorescence	<i>Gerbig et al.</i> [1999]
	O ₃	UV absorption	Thermo Electron Co. Model 49
DLR Falcon	CO	VUV fluorescence	<i>Gerbig et al.</i> [1996]
	O ₃	UV absorption	<i>Schlager et al.</i> [1997]
MOZAIC	CO	improved IR correlation	<i>Nedelec et al.</i> [2003]
	O ₃	UV absorption	<i>Marenco et al.</i> [1998]

^aThe NOAA-P3 O₃ instrument is a new installation, but similar to the one described in the listed reference.

^bM. A. Avery et al., FASTOZ: An accurate, fast-response in situ ozone measurement system for aircraft campaigns, submitted to *Journal of Atmospheric and Oceanic Technology*, 2006.

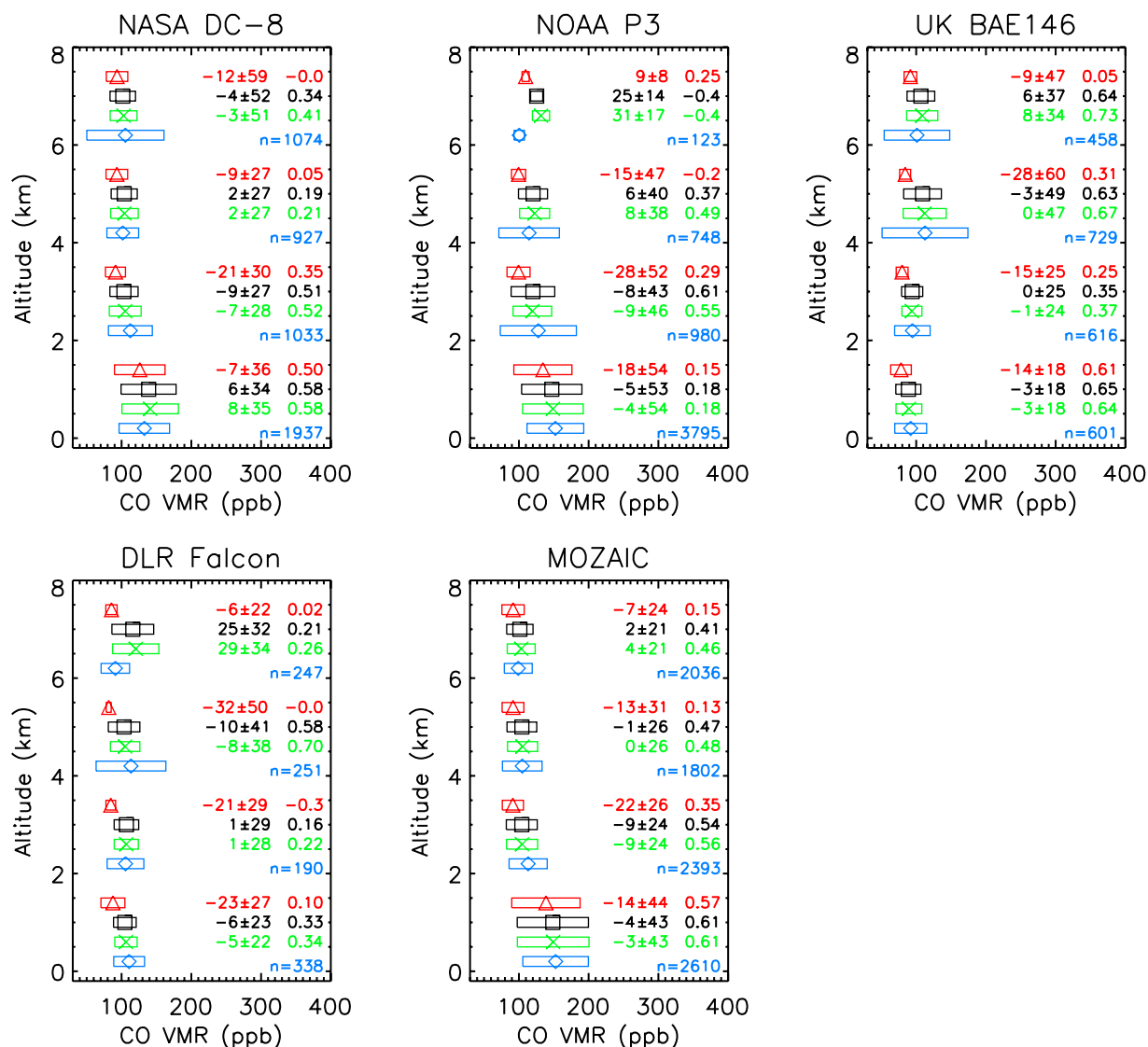


Figure 1. Model evaluation with aircraft data for CO (blue diamonds: observations; green crosses: model with fire emissions injected over 0–9 km; black squares: model simulations with fire emissions injected at surface; red triangles: no fire emissions). The mean percent bias and standard deviation (model minus measurement), correlation coefficient r and number of data points for 2-km wide altitude bins are specified.

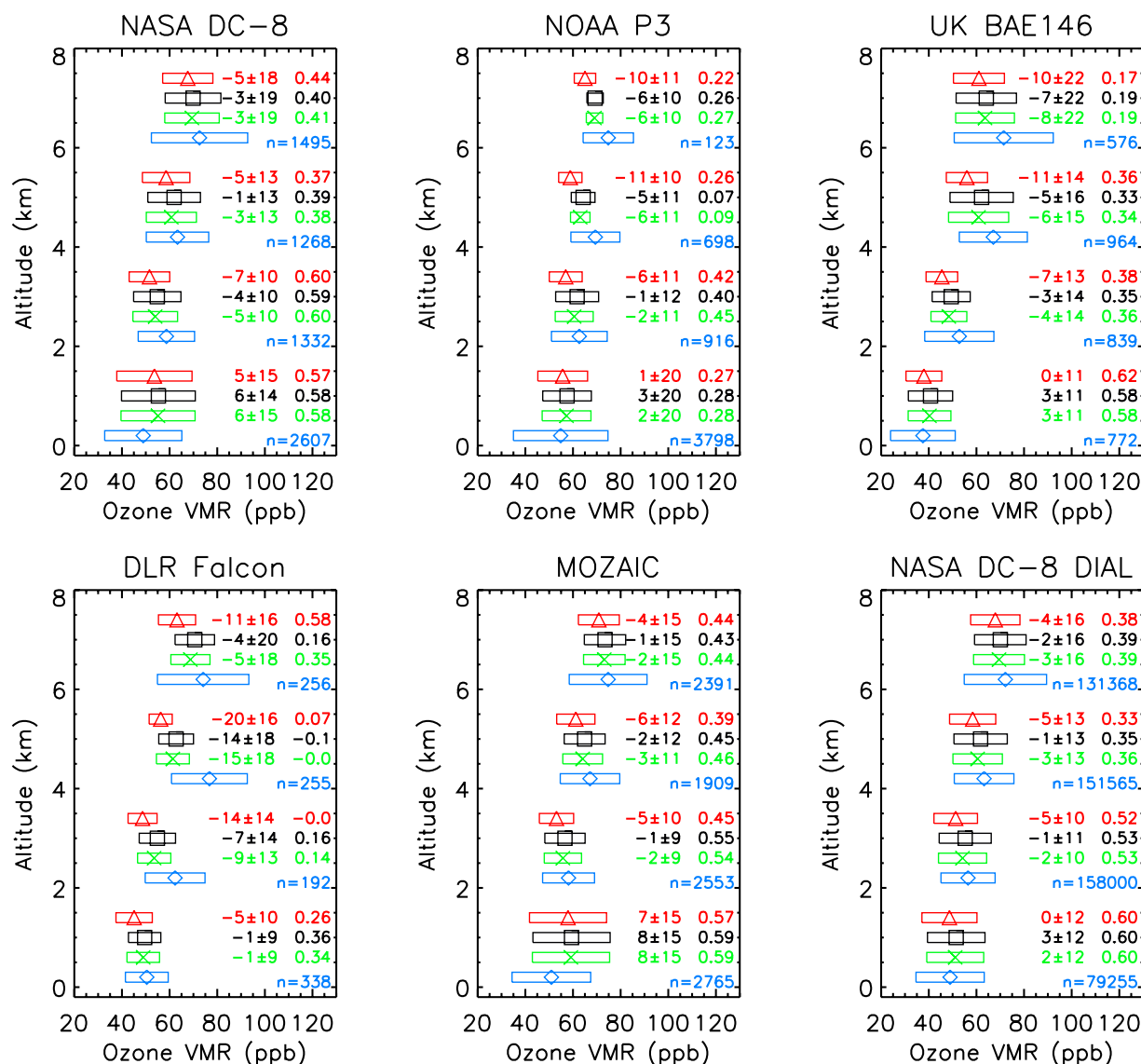


Figure 2. As in Figure 1, but for O_3 .

analysis we perform using O_3^{NOx} in this study is expected to give a comparable accuracy.

3. Model Evaluation

[12] MOZART-4 simulations (BBsrf and BBvert) have been evaluated by comparison with aircraft measurements taken in the framework of the ICARTT campaign during summer 2004. Table 1 includes a list of the platforms, instrumentation, and corresponding references. Measurements with the NASA DC-8 covered large parts of North America and the Northern Atlantic, the NOAA-P3 flights were focused on the Eastern United States, the British BAE146 performed most flights over the Atlantic, and the German Falcon covered mostly Europe. The Measurements of Ozone aboard Airbus In-service Aircraft (MOZAIC) data set has global coverage, but we are including only measurements over North America, the Northern Atlantic and Europe in accordance with the regions covered by the other aircraft. Most low-altitude measurements for this data set

are from take-offs and landings over airports in Europe and the US. For a more detailed description of all flight patterns we refer to F. C. Fehsenfeld et al. (International Consortium for Atmospheric Research on Transport and Transformation (ICARTT): North America to Europe: Overview of the 2004 summer field study, submitted to *Journal of Geophysical Research*, 2006).

[13] For the comparison of the model with the observations, 2-hour average model data have been linearly interpolated to the time and location of the aircraft data. The time resolution of the observations is 1 min. The results for BBvert, BBsrf, and for comparison, noBB, are shown in Figure 1 for CO and in Figure 2 for O_3 , respectively. Statistics have been calculated for the individual aircraft data sets and binned onto a 2-km wide altitude grid. These values are specified in the figures. The agreement with observations for CO as well as O_3 is generally better in the simulations with fires than in the simulation without fires. CO and O_3 mixing ratios are clearly different between the BB and noBB simulations for all platforms, also for the UK

Table 2. Statistics Over the Altitude Range 0–8 km for the Model Simulations BBSrf, BBvert, and noBB and the Platforms Listed in Table 1^a

	BBSrf	BBvert	noBB	BBSrf to noBB	BBvert to noBB	BBSrf to BBvert
<i>CO (ppbv) Mean and Standard Deviation</i>						
DC-8	119 ± 37	117 ± 35	106 ± 31	<0.01	<0.01	0.01
P-3	140 ± 41	139 ± 41	124 ± 39	<0.01	<0.01	0.07
BAE146	100 ± 24	99 ± 23	84 ± 13	<0.01	<0.01	0.14
Falcon	110 ± 24	108 ± 23	85 ± 11	<0.01	<0.01	0.06
MOZAIC	117 ± 39	116 ± 39	105 ± 36	<0.01	<0.01	0.06
<i>O₃ (ppbv) Mean and Standard Deviation</i>						
DC-8	59 ± 14	60 ± 14	57 ± 14	<0.01	<0.01	0.02
P-3	59 ± 10	59 ± 10	57 ± 10	<0.01	<0.01	<0.01
BAE146	51 ± 14	52 ± 15	48 ± 12	<0.01	<0.01	<0.01
Falcon	58 ± 11	59 ± 11	53 ± 10	<0.01	<0.01	0.01
MOZAIC	62 ± 13	63 ± 13	60 ± 13	<0.01	<0.01	<0.01
DIAL	54 ± 8	56 ± 9	53 ± 8	<0.01	<0.01	<0.01

^aMean and standard deviation for CO and O₃ concentrations and the significance level of the student's T-statistics comparing BBSrf to noBB, BBvert to noBB, and BBSrf to BBvert are shown.

BAE146 and DLR Falcon. This indicates that plumes from the Alaska and Canada fires reached all the way to Europe. We list statistics for modeled CO and O₃ concentrations for the different platforms in Table 2. The data included in the statistics corresponds to those shown in Figures 1 and 2, but determined for the entire altitude range from the surface to 8 km. The T-test significance levels for simulations with and without fire emissions are above 99% for all platforms indicating the samples have significantly different means. It is interesting to note that the T-test statistics comparing BBvert and BBSrf show a somewhat higher significance level for O₃ compared to CO. This suggests the modeled O₃ production from the fires is slightly more sensitive to the injection height than the concentration fields of CO.

[14] For most altitudes and platforms, the CO bias between model and observations is less than 10% for both BBSrf and BBvert (see Figure 1). The mean bias as well as the correlation improved upon adding fire emissions into the model, with the only exception being the highest-altitude bin for the NOAA P3 and DLR Falcon data set. We believe this can partly be explained by the small data sample in these bins, and, associated with that, the comparison is more strongly impacted by single events. This might also contribute to the large bias in the 4–6 km bin for the DLR Falcon. The comparison for O₃ (Figure 2) shows an agreement of better than 10% for all platforms and altitude bins when fire emissions are included in the simulations. No clear conclusion can be drawn from the evaluation if either BBSrf or BBvert lead to better general agreement. The comparison for individual fire plumes give a better agreement for either the one or the other simulation. This reflects the combination of crown, smoldering, and peat burning of the Alaska fires. The two cases we ran do not represent the full complexity of fire behavior, but are probably better regarded as sensitivity tests to the vertical distribution of emissions.

4. Impact of Biomass Burning on CO and O₃ at PICO-NARE

[15] For the analysis of the O₃ production from the wildfires in Alaska and Canada we made use of in situ measurements at the PICO-NARE station. The station is

located on the summit caldera of Pico mountain on Pico Island in the Azores, Portugal (2225 m above sea level, 38.47N, 28.40W) and is well suited for studying North American pollution outflow. Air masses at this location typically arrive from North America, but frequently originate from high-latitude regions such as Alaska and Siberia [Honrath *et al.*, 2004], often with enhancements in CO and O₃ that have been attributed to boreal fire impacts [Lapina *et al.*, 2006]. The advantage of measurements at PICO-NARE compared with other locations on the continent is its remote location allowing the sampling of chemically well processed air masses.

[16] CO at PICO-NARE was measured using a nondispersive infrared absorption instrument (Thermo Environmental, Inc., Model 48C-TL) modified as described by Parrish *et al.* [1994]. O₃ was measured with a commercial ultraviolet absorption instrument (Thermo Environmental Instruments Inc., Franklin, Massachusetts, Model 49C). Data are available as 1-min averages. For the 2-hour averages used in this study the precision for CO is estimated to be better than 9 ppbv and for O₃ better than 1 ppbv. For a description of the station and the measurement techniques we refer to Honrath *et al.* [2004] and Owen *et al.* [2006].

[17] For comparing the model simulations with the observations at PICO-NARE, the observations have been averaged in time to match the 2-hour window of the simulations, and the model data have then been linearly interpolated to the location and pressure level of the observations. Because of the coarse model resolution, the simulations do not resolve upslope events occurring at the mountain site. Observations potentially affected by upslope flow were small during summer 2004. We identified these periods as described by Kleissl *et al.* [2007] and omitted them from the analysis.

[18] Figure 3 shows the time series for modeled and measured CO and O₃ at PICO-NARE. In addition to results from the BB model simulations, we also include results from the noBB simulation to emphasize the impact of the Alaskan/Canadian wildfires. For clarity, we reduced the temporal resolution in the graphs to daily average values, however, our analysis refers to the 2-hour average values. A detailed analysis of PICO-NARE 30-min observations in the 2004 fire season is provided by Val Martin *et al.* [2006]. As can be

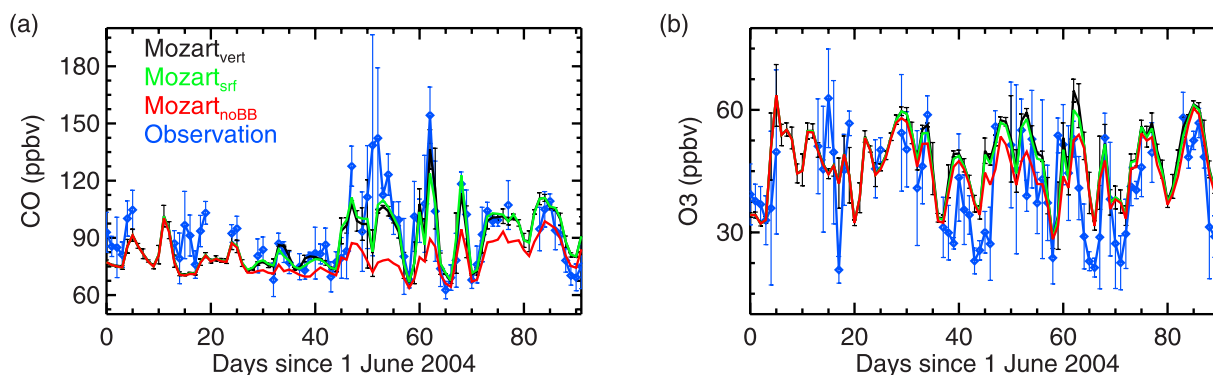


Figure 3. Measured and modeled time series of CO and O₃ mixing ratios at PICO-NARE (daily averages are shown).

seen in Figure 3, the model closely matches the observed temporal variability, and also captures the magnitudes fairly well. The mean bias between modeled (BBsrf) and observed mixing ratios is -3 ± 16 ppbv for CO and 6 ± 12 ppbv for O₃. The corresponding biases for the simulation without fire emissions are -12 ± 19 ppbv for CO and 4 ± 12 ppbv for O₃, respectively. Daily CO fire tracers in the model estimate a typical transport time on the order of 1–2 weeks for biomass-burning plumes reaching PICO-NARE.

[19] The time series for CO from the simulations BB and noBB indicate a clear impact from the fires at PICO-NARE throughout the months of July and August with the most extreme period from the end of July to mid-August. This is a combination of the most intense fire activity occurring in mid to end of July [Pfister et al., 2005] and the transport time of 1–2 weeks. The period from 22–24 July had the highest half-hour average CO levels yet recorded at the PICO-NARE station [Val Martin et al., 2006]. The impact of the fires on the O₃ concentrations is less pronounced, but differences between BB and noBB of up to 10 ppbv are evident during some of the intense episodes. The difference in CO and O₃ concentrations by subtracting noBB from BBsrf gives an average enhancement due to the fires of 8 ppbv (8%) for CO and 2 ppbv (4%) for O₃.

[20] The correlation between the CO mixing ratios from the simulation BBsrf and the observations is $r = 0.64$ compared to a correlation of $r = 0.48$ between noBB and the observations. During times of intense biomass-burning impact, the noBB run actually shows slight enhancement in the CO concentrations as well, indicating that these outflow events transported pollution from the fires together with elevated pollution from likely North American anthropogenic sources.

[21] The correlation between the measured and modeled O₃ is $r = 0.51$ for the simulation noBB and increases only slightly for the BB runs ($r = 0.54$), an indication of the less pronounced or more complex [Val Martin et al., 2006] effect of the fires on the O₃ burden compared to the CO burden. While the model is picking up the higher O₃ values moderately well, neither the BB nor the noBB simulations capture the low end of the observed O₃ concentrations. This is likely due to the positive O₃ bias in the model over the US, leading to an overestimate of North American outflow of O₃ and to an overestimate in the modeled O₃ mixing ratio of maritime background air. In agreement with the conclusions drawn

from the model evaluation in section 3 it cannot be stated if either BBsrf or BBvert results in better agreement with the observations. Unless otherwise mentioned, we will focus in the following analysis on results for BBsrf.

5. Ozone Production from Boreal Fires

[22] Assuming a linear relationship between CO emissions and net O₃ production, the relationship between tropospheric CO and O₃ concentrations might be used as an estimate for the net O₃ production in regional plumes [Parrish et al., 1993; Forster et al., 2001]. The enhancement ratio $\Delta O_3/\Delta CO$ is defined as the difference between the O₃ concentrations in a polluted air mass from that of background air, normalized by the excess mixing ratio of CO. In the case of biomass-burning plumes, the background defines concentrations of CO and O₃ not linked to the fire emissions.

[23] The change in the Northern Hemispheric net O₃ production rate due to the fires, calculated by differencing net O₃ production rates in the BB and the noBB simulation, is estimated as 6 Tg O₃ for June through August. This is contribution of 3% to the Northern Hemispheric net ozone production. Normalizing by the total CO emissions for this time period (30 ± 5 Tg CO) yields a global average enhancement ratio for the fires in Alaska and Canada of 0.12 ppbv/ppbv. In the following sections we examine the feasibility of estimating the O₃ production of North American boreal fires by using enhancement ratios based on observed and modeled mixing ratios of CO and O₃ at PICO-NARE.

5.1. Determining the Enhancement Ratio from CO and O₃ Observations

[24] There are two common ways to calculate $\Delta O_3/\Delta CO$. The first, in the following referred to as the “scatter technique”, determines the enhancement ratio from the slope of the linear fit of O₃ versus CO mixing ratios [Parrish et al., 1993]. The second, termed as “enhancement technique”, infers “background” concentrations of CO and O₃ from air masses not affected by the considered pollution source (in our case the wildfires in Alaska and Canada) and calculates the corresponding excess mixing ratios by subtracting background concentrations from total concentra-

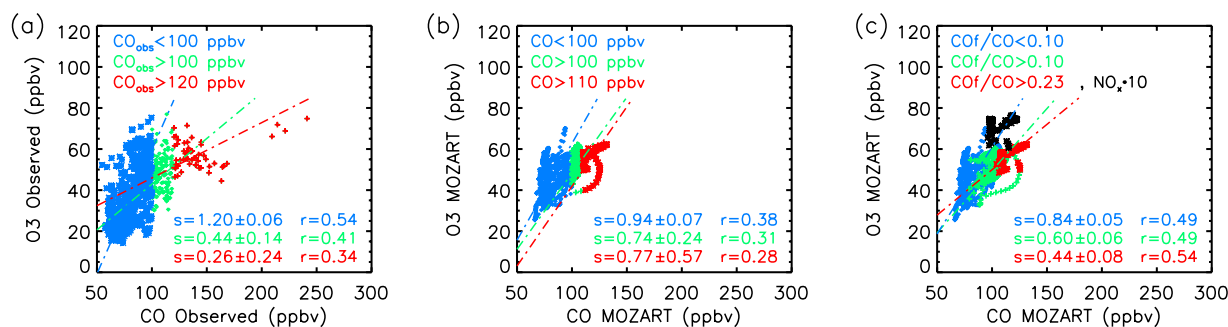


Figure 4. (a) Observed and (b, c) modeled CO-O₃ relationships at PICO-NARE. Air masses are separated into three groups: mostly non-fire-related origin (blue); some biomass-burning impact (green); pronounced biomass-burning impact (red). In Figure 4c, results are also shown for a simulation where the NO_x fire emissions were increased by a factor of 10.

tions [Mauzerall *et al.*, 1998]. Both methods are discussed in the following.

5.1.1. Scatter Technique

[25] This technique has been applied in Figure 4 showing CO-O₃ scatter plots for observed and modeled concentrations at PICO-NARE. The data were grouped into air masses with varying biomass-burning impact by using the magnitude of the observed CO mixing ratio as the threshold. Studies by Honrath *et al.* [2004] and Lapina *et al.* [2006] show that periods of extreme summertime CO concentrations frequently coincide with airflow from Northern latitudes transporting pollution from wildfires in Siberia, Alaska and Canada to PICO-NARE. To allow comparison with the observations, we applied two methods to the model data: (1) we used a threshold derived from the simulated CO and (2) we used the relative contribution of the fire tracer CO_f. The second method gives in some sense the true solution, as it is not impacted by sources of high CO other than the wildfires. The thresholds, specified in the graphs, were chosen in a way that the number of data points was roughly equal in the different subsets. The coarse spatial resolution in the model results in a more pronounced dilution of biomass-burning plumes and this explains the smaller threshold in total CO applied to the subset of high intense plumes in the model compared to the observations.

[26] The fitting technique applied is a reduced major axis reduction (RMA). It uses the geometric mean of the slopes of the standard linear regression of *y* versus *x* and of *x* versus *y* [Draper and Smith, 1998] thus taking into account the variability in both abscissa and ordinate. The mean slope and the corresponding standard deviation are specified in Figure 4.

[27] The scatter in the data and the uncertainties in the slopes are explained by the mixture of different air masses, variability in the background CO and O₃ levels, and differing pathways and photochemical ages in the sampled plumes. The slopes are also somewhat dependent on the fitting technique applied. The calculated $\Delta O_3/\Delta CO$ is independent of air mass age if the tracers used have similar lifetimes or have lifetimes much longer than the transport time, but this assumption is not entirely fulfilled in the case of CO and O₃. However, in a statistical sense, a clear distinction between the different types of air masses is evident with the smallest O₃ enhancements per unit CO for the most intense plumes in both model and data. The

decrease in the slopes with increasing biomass-burning impact is seen in both the model data (Figure 4b) and the observations (Figure 4a). However, the model does not capture the measured $\Delta O_3/\Delta CO$ due to the impact of mixing in the model. As a result, the calculated slope has a rather large value with, at the same time, a high uncertainty. Applying the ratio CO_f/CO as a selection criteria instead (Figure 4c) we achieved a clearly stricter separation of the fire impact for the modeled plumes. The slope calculated for the most biomass-burning-impacted subset is then 0.44 ± 0.08 with a correlation of $r = 0.54$ instead of a slope of 0.77 ± 0.57 and a correlation of $r = 0.28$ when applying total CO mixing ratios as threshold. This slope is still higher than the observed one and this is likely due to more strongly diluted plumes in the model resulting from the coarse spatial resolution. As will be shown in section 5.2, the selection of more intense model fire plumes reduces the estimated slope.

[28] The generally higher slopes for air masses least impacted by biomass-burning sources (defined as “nonfire plumes” here and characterized strongly by anthropogenic pollution sources) compared to those more strongly impacted by the wildfires is consistent with earlier studies [Wofsy *et al.*, 1992; Andreae *et al.*, 1994; McKeen *et al.*, 2002] and have been explained by a lower NO_x:CO emission ratio in boreal fires relative to urban and industrial sources. In Figure 4c we include results from a simulation where the NO_x:CO emission ratio for the wildfire emissions in the model was increased by a factor of 10 to match the emission ratio of anthropogenic sources. The pronounced difference between air masses with weak and with strong biomass-burning impact is diminished in this case supporting the hypothesis that the difference between O₃ production of anthropogenic and biomass-burning plumes can largely be explained by a difference in NO_x:CO emission ratios.

[29] It is evident from Figure 4 that the limitations used in the selection of biomass-burning-impacted air masses and the degree of mixing in the considered air masses have an effect on the calculation of $\Delta O_3/\Delta CO$. The observed and modeled correlations also indicate that the enhancement ratio decreases the more strict the selection criteria applied are, and this dependence will be looked into more closely in section 5.2.

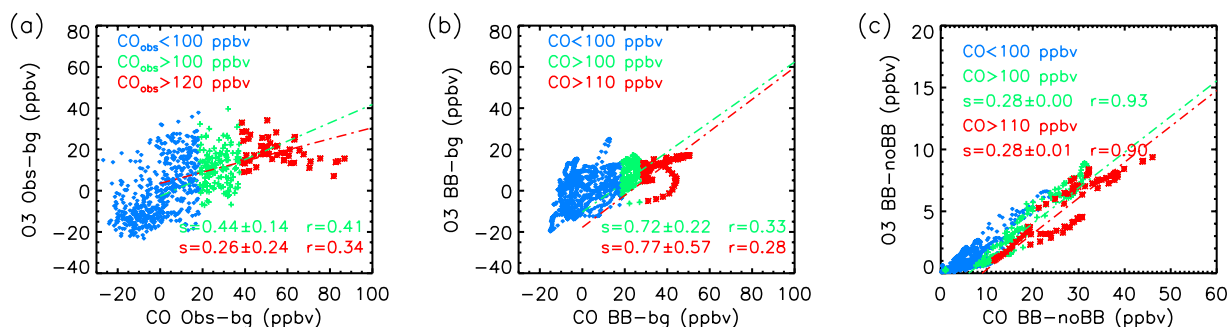


Figure 5. (a) Observed and (b, c) modeled CO-O₃ excess mixing ratios. In Figures 5a and 5b a constant background (bg) is calculated from the subset of non-fire-impacted airmasses; in Figure 5c the background is derived from the noBB simulation.

5.1.2. Enhancement Technique

[30] The enhancement technique requires knowledge of the background concentrations, and large uncertainties might be introduced if the background and its variability are not well known. For modeling studies, however, the variability in background concentrations can be determined accurately from a simulation where the considered emission source is omitted.

[31] Figure 5 shows observed and modeled excess mixing ratios of O₃ versus CO for the air mass separation applied earlier (section 5.1.1). For Figures 5a and 5b we estimated the background by averaging CO and O₃ mixing ratios over the subset of non-fire-impacted air flow, which explains the existence of negative excess mixing ratios in this subset of data. For the observations the derived background values are 82 ppbv for CO and 37 ppbv for O₃; for the model data we obtain 81 ppbv for CO and 45 ppbv for O₃. The derived slopes for the air masses impacted by biomass burning are nearly identical to the values derived from the scatter technique showing that the background value we assumed in the enhancement technique is similar to the one implied in the scatter technique. The difference in the slopes for observed and modeled CO-O₃ relationships (Figures 5a and 5b) suggests this method is also sensitive to the amount of mixing.

[32] Figure 5c shows modeled slopes when the background is estimated from the simulation without fire emissions. In some sense, this is the result one would obtain assuming perfect data, i.e., if the excess mixing ratios of CO and O₃ are precisely known. For each data point in the BBsrf simulation a corresponding background value is derived from the noBB run, thus the temporal variability in the background is accounted for. The standard deviation of the background mixing ratios as determined from the noBB simulation is on the order of 5 ppbv for the biomass-burning plumes. Compared to the scatter technique and the enhancement technique with a constant background, the excess mixing ratios for CO and O₃ derived with this technique are more strongly correlated and the calculated slopes are much less sensitive to the selection of the air mass. $\Delta\text{O}_3/\Delta\text{CO}$ for the biomass-burning plumes at PICO-NARE derived from this technique is 0.28 ppbv/ppbv when the air masses are filtered for the points most impacted by biomass burning, and 0.23 ppbv/ppbv for all data points. These values are lower than those calculated with the scattering technique for the model data and match the

observed $\Delta\text{O}_3/\Delta\text{CO}$. This concludes that the modeled fire plumes are more diluted compared to observed plumes because of the coarse model resolution, and still carry characteristics of non-fire-related pollution. This impact only cancels out by considering the contribution of time-varying non-fire-related background air. When the sensitivity to model mixing is removed, the model captures the observed enhancement ratio.

[33] Thus provided accurate information about the variability in the background levels is available, the enhancement technique allows a more accurate determination of $\Delta\text{O}_3/\Delta\text{CO}$ than the scatter technique. The same technique applied to the model simulation in which the NO_x fire emissions were increased by a factor of 10 yields slopes on the order of 0.8, i.e., close to the enhancement ratio estimated for anthropogenic sources.

5.2. Enhancement Ratios and O₃ Production

[34] We used the model data to test the sensitivity of $\Delta\text{O}_3/\Delta\text{CO}$ derived with both the scatter and the enhancement techniques to the degree to which air masses are impacted by biomass burning. For the enhancement technique the background was derived from the noBB simulation. Figure 6 shows $\Delta\text{O}_3/\Delta\text{CO}$ as a function of the magnitude of biomass-burning impact indicated by selecting air masses based on a lower limit of the fraction of CO_f to total CO. The enhancement technique shows a weak dependence on the selected air masses, and the variations seen

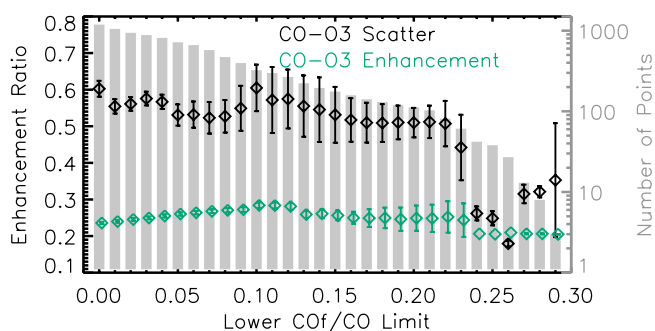


Figure 6. Enhancement ratio (mean slope and standard deviation) determined by the scatter and the enhancement technique as a function of intensity of biomass-burning influence of considered air masses. The number of selected data points is represented by the shaded area. Results for the BBsrf simulation.

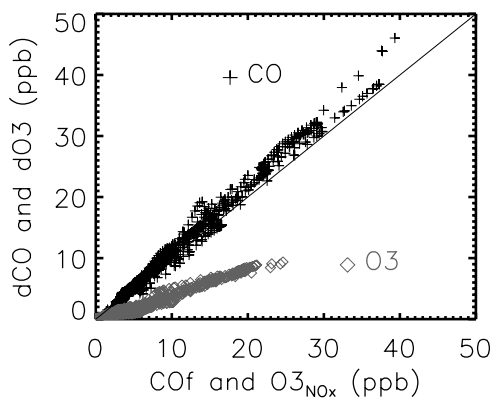


Figure 7. Correlation between the model fire tracers CO_f and $\text{O}_3^{\text{NO}_x}$ and the difference in CO and O_3 mixing ratios between the simulations BBsrf and noBB (defined as $d\text{CO}$ and $d\text{O}_3$) at PICO-NARE.

reflect the variability in O_3 production in biomass-burning plumes due to changes in O_3 chemistry, transport pathways and times, and a combination of these or more processes. The average $\Delta\text{O}_3/\Delta\text{CO}$ is calculated as 0.25 ppbv/ppbv for BBsrf and a slightly higher value, 0.27 ppbv/ppbv, is calculated for BBvert. This value is close to the enhancement ratio of 0.26 derived from the observations when intense plumes are selected only (Figure 4).

[35] Our values for $\Delta\text{O}_3/\Delta\text{CO}$ are in the range of values found in the literature. Mauzerall *et al.* [1996] calculated enhancement ratios for aged boreal fire plumes on the order of 0.1 ± 0.2 ppbv/ppbv. A value of 0.1 ppbv/ppbv was encountered during SOS-95 by Wotawa and Trainer [2000] and similar values during ABLE-3 for Alaska fires [Jacob *et al.*, 1992]. McKeen *et al.* [2002] report enhancement ratios of 0.17 ppbv/ppbv. Higher averaged enhancement ratios are estimated by Bertschi and Jaffe [2005] and Honrath *et al.* [2004] for highly aged boreal fire plumes: 0.4 ppbv/ppbv and 0.7 ppbv/ppbv, respectively.

[36] In the case of the scatter technique it is evident that $\Delta\text{O}_3/\Delta\text{CO}$ is higher for the weakly impacted plumes due to the mixing of the biomass-burning impact with the impact of other pollution sources. As mentioned earlier, during times of intense fire plumes, increased pollution was also transported to PICO-NARE (Figure 3). The average O_3 concentration for the noBB simulation is 44 ± 9 ppbv for $\text{CO}_f/\text{CO} < 0.01$, but 47 ± 5 ppbv and 47 ± 4 ppbv for $\text{CO}_f/\text{CO} > 0.1$ and $\text{CO}_f/\text{CO} > 0.2$, respectively. Corresponding CO concentrations are 77 ± 8 ppbv, 84 ± 6 ppbv, and 82 ± 6 ppbv. When air masses with at least 20% biomass-burning impact are selected, the slopes calculated with the two different techniques approaches a similar range. However, toward stricter limitations the number of data points is small and the fitting technique is less reliable.

[37] By using $\Delta\text{O}_3/\Delta\text{CO} = 0.25$ ppbv/ppbv as derived from the enhancement technique, an approximation for the total O_3 produced from the fires can be made [Parrish *et al.*, 1993; Mauzerall *et al.*, 1996]. With 30 ± 5 Tg CO emitted by the fires from June through August as stated by Pfister *et al.* [2005], an O_3 production of 10.7–15 Tg O_3 is estimated for the same time period (30 ± 5 Tg CO

multiplied by 0.25 ppbv ppbv $^{-1}$ and corrected by the ratio of O_3 (48 g mol $^{-1}$) to CO (28 g mol $^{-1}$) molecular weights).

[38] This value is larger than the Northern Hemispheric net chemical production rate of 6 Tg O_3 in the model as mentioned earlier. The discrepancy can be explained in that $\Delta\text{O}_3/\Delta\text{CO}$ at the location of PICO-NARE is not representative for the total net change in O_3 , but rather for the net O_3 production rate covering the region from the source location to the Azores. Close to the source region net chemical production of fire-related O_3 dominates, while further downwind from the source (e.g., Europe and Asia) net chemical loss dominates. The modeled net O_3 production calculated over a region representative for air masses reaching PICO-NARE (stretching from 180W to 20W and from 40N to 70N) is 9 Tg O_3 for BBsrf and 11 Tg O_3 for BBvert, i.e., in the range of the estimate based on $\Delta\text{O}_3/\Delta\text{CO}$. These results demonstrate that the measurements and model simulations at the location of PICO-NARE being representative of aged biomass-burning plumes indeed give a good measure of the O_3 production of fires in North America. Differences between the $\Delta\text{O}_3/\Delta\text{CO}$ based estimate and the model calculated production are explained by uncertainties in the calculation of the slopes and differing pathways and chemical ages for plumes reaching PICO-NARE.

[39] As mentioned earlier, our model simulations not only include a CO fire tracer, but also an O_3 fire tracer $\text{O}_3^{\text{NO}_x}$ that tracks the amount of O_3 produced from the NO_x fire emissions. One might assume that the global net O_3 production for this tracer equals the amount derived when subtracting results for simulations with and without fire emissions as has been done above (6 Tg O_3). However, the net O_3 production rate for the Northern Hemisphere calculated from the O_3 fire tracer is higher, close to 9 Tg O_3 . The reasons for this are due to the nonlinearity in O_3 chemistry and are explored in the following section.

5.3. Changes in the O_3 Chemistry Due to Fire Emissions

[40] In Figure 7 we show correlations between the model CO and O_3 fire tracers and the difference in O_3 and CO mixing ratios from BBsrf and noBB simulations defined as $d\text{O}_3$ and $d\text{CO}$, respectively. As can be seen, the correlation for CO is close to the 1:1 line, but for O_3 the mixing ratios of $\text{O}_3^{\text{NO}_x}$ are clearly larger compared to $d\text{O}_3$ indicating that O_3 production related to the fires must have been offset by an increased loss of O_3 .

[41] To explore the mechanisms behind the O_3 production from the fire emissions, we compared O_3 concentrations, production and loss terms in the model for the simulations BBsrf and noBB. The data set has been split into three groups of varying fire impact determined by the ratio CO_f/CO . Statistics for the individual subsets are plotted in Figure 8. The maps (Figure 8a) denote the geographical coverage of the selected data with red indicating a high, and blue a low, concentration of data points. The most intense plumes are concentrated near the source location, but plumes of high fire impact can also be seen all the way to Europe. The high-intensity plumes are mostly located near the surface (Figure 8b) as expected when the emissions are released at the lowest model level. With time, atmospheric transport and convection spread plumes over a larger altitude range.

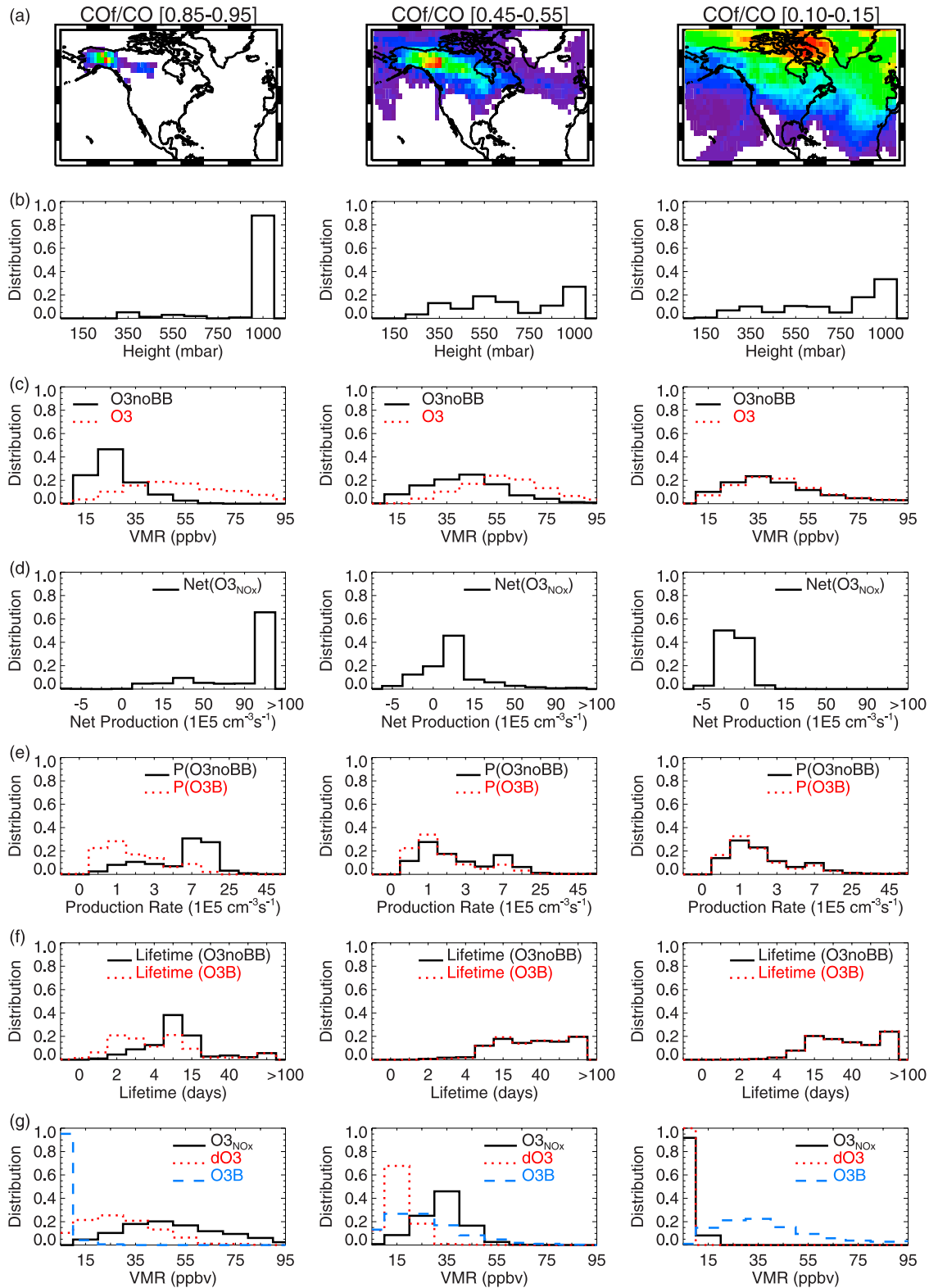


Figure 8. Statistics for ozone concentrations and ozone production and loss terms for three different subsets of fire plume intensity as characterized by the ratio of CO_f/CO . (a) Spatial distribution for selected data points. (b) Frequency distribution for the height of the selected data points. (c) Frequency distribution of the volume mixing ratios O_3noBB and O_3 . (d) Net O_3 production rate for the fire tracer $\text{O}_3^{\text{NO}_x}$. (e) Frequency distribution of the O_3 production rate for O_3noBB and O_3B (background O_3 estimated by subtracting O_3 and $\text{O}_3^{\text{NO}_x}$). (f) As in Figure 5e but for the chemical lifetime. (g) Frequency distribution of the volume mixing ratios $\text{O}_3^{\text{NO}_x}$, $d\text{O}_3$, and O_3B .

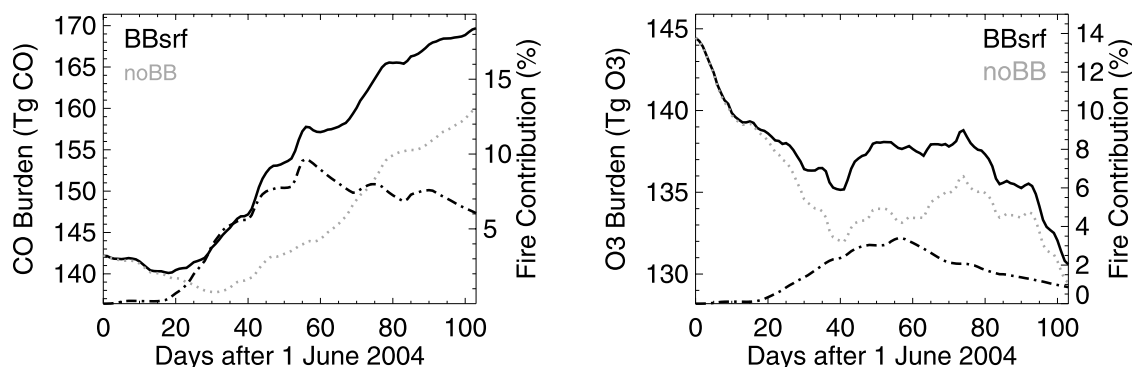


Figure 9. Northern Hemispheric burden of CO and O₃ for the altitude range surface – 300 mbar. Model results for simulations BBsrf (solid line) and noBB (dotted line). The dash-dotted line denotes the percentage difference between simulations BB and noBB (shown on the secondary ordinate).

[42] Figure 8c shows that O₃ levels without fire emissions (O₃noBB) are mostly below 40 ppbv over the source regions; that is, the fires occurred in an area of low O₃ concentrations. The additional NO_x from the fires causes a shift in the distribution of O₃ concentrations toward higher values. The effect is most pronounced over the source region, but a slight positive shift is also evident for the subset of least impacted plumes.

[43] The increase in O₃ is caused by a strong net production of the fire tracer O₃^{NOx} in the most impacted plumes with the magnitude decreasing with decreasing plume intensity. This is shown in Figure 8d where we illustrate histograms for the O₃^{NOx} net chemical production. Even though the strongest production takes place close to the source region, continuing production is also evident in regions further downwind from the source. For the subset of least impacted plumes (and most aged plumes), there are a significant number of data points with net chemical loss of O₃^{NOx}.

[44] Figures 8e to 8g show the changes to background O₃ levels when fire emissions are injected into the system. Figure 8e denotes the distribution for production of O₃noBB and of background O₃ with fire emissions; the latter defined as O₃B. O₃B is calculated by subtracting the O₃ fire tracer from the total O₃. The production of O₃B is less than the production of O₃noBB. Thus by adding fire emissions to the system, the production of background O₃ is reduced in the simulations. This is explained by reduced background production of peroxy radicals (not shown here). Peroxy radicals play an important role in ozone production by reacting with NO to form NO₂ which then is photolyzed to give atomic oxygen necessary in the O₃ formation. Changes are most pronounced over the source region, but differences are also evident in less impacted plumes.

[45] In addition to a reduced production of O₃B, the loss of O₃B is increased over that of O₃noBB, reflected in a reduction in the chemical lifetime (Figure 8f). The reduced production and increased loss of background O₃ result in lower concentrations of O₃B compared to O₃noBB. In Figure 8g we show the corresponding frequency distributions for O₃^{NOx}, O₃B and dO₃. When compared to Figure 8c, we see that over the source region, O₃B has on average ~80% smaller values compared to O₃noBB, and most of the O₃ present is in the form of O₃^{NOx}, i.e., O₃ due to the NO_x fire emissions.

[46] The strong reduction of background O₃ levels when fire emissions are included explains why concentrations of O₃^{NOx} are larger than the difference in O₃ concentrations between runs with and without fire emissions. In contrast, the CO chemistry has a first-order linearity, thus the concentrations of the fire tracer CO_f are close to the difference of CO concentrations simulated with and without fire emissions (Figure 7). However, the fires also impacted background levels of atmospheric CO to some extent. The high VOC and CO emissions from the fires result in a reduction in average OH concentrations. This in turn reduces the rate of oxidation of CO and results in increased background CO levels. This increase has been estimated in the model by comparing the background CO with fire emissions (calculated by subtracting CO_f from total CO concentrations in BBsrf) to the CO field without fire emissions. For the Northern Hemisphere we calculate an increase in the burden of background CO of up to 1 Tg CO.

5.4. Impact of Alaska/Canada Wildfires on the O₃ Budget

[47] Finally, using the model results, we examine how increases in the CO and O₃ concentration fields related to the wildfires affected the Northern Hemispheric and the regional trace gas budgets. In Figure 9 we show the time series for the modeled Northern Hemispheric CO and O₃ burden (surface –300 hPa) and the changes related to the emissions from the fires. The change in the CO burden reaches close to 10% around the end of July. The corresponding changes in the O₃ burden are on the order of up to 4%. On average the Northern Hemispheric CO and O₃ burdens during the summer 2004 were increased because of emissions by the fires by 4–5% and 2%, respectively.

[48] As expected, the largest changes in the atmospheric burden occurred over Alaska and Canada (50–70N, 180E–60W) with an average increase in the O₃ burden of 7–9% for the altitude range surface –300 hPa, and 11–12% for the range surface –800 hPa. For comparison, over the altitude range up to 300 hPa, this is slightly smaller than the estimated contribution of stratospheric O₃ (11%) in the model, but for the range up to 800 hPa exceeds the contribution of stratospheric O₃ (3%).

[49] Because of the transport of O₃ and its precursors, effects from the fires are also expected far downwind of the

source location. Over Europe (35–70N, 20W–20E) we estimate a contribution of O₃ from the fires of up to 10% around the end of July for the surface –300 hPa range and up to 8% for the range surface –800 hPa. Averaged over the summer, the contributions are on the order of 3% for both altitude ranges considered. These results show that even though the fires had a rather small contribution to the large-scale hemispheric budget of O₃, over certain regions and altitudes, even far downwind from the source itself, the impact is significant.

6. Conclusion

[50] We have determined the amount of O₃ produced from the wildfires in Alaska and Canada in summer of 2004 by using a combination of model simulations and observations. The modeled CO and O₃ fields have been evaluated by comparison with a comprehensive set of aircraft measurements taken during the ICARTT campaign.

[51] In analyzing the O₃ production from North American boreal fires we used measured and modeled CO and O₃ mixing ratios at the PICO-NARE station in the Azores. The results show that the enhancement ratio $\Delta\text{O}_3/\Delta\text{CO}$, defined as the increase in O₃ per unit increase in CO, derived from observed and modeled concentrations at PICO-NARE is a good measure for the O₃ production from the Alaska and Canada fires. However, we also show that this measure can be very sensitive to the selected air masses. Our analysis yields enhancement ratios of 0.25 ppbv/ppbv for aged plumes of Alaskan and Canadian wildfires, which is in the range of values found in the literature. The enhancement ratio found for boreal biomass-burning plumes is about a factor of 3–4 smaller than that of anthropogenic plumes. We have also performed a sensitivity simulation that clearly showed that the difference in the enhancement ratio for anthropogenic and boreal fire biomass-burning plumes is a result of the difference in the NO_x/CO emissions ratios for these sources.

[52] Controversies exist in the understanding of the importance of O₃ production from boreal forest fires. The total net O₃ production from the boreal fires in Alaska and Canada in the summer of 2004 in our model is estimated as 6 Tg O₃ which gives a contribution of about 3% to the Northern Hemispheric budget. Considering only a region spanning from the source to the Azores, a net chemical production of 9–11 Tg O₃ is calculated in the model. This is in agreement with the estimate derived from enhancement ratios based on model simulations and observations at PICO-NARE (10.7–15 Tg O₃). Large increases in the O₃ burden are observed downwind of the fires because of transport of O₃ produced near the fires as well as continuing O₃ production in the fire plumes. Modeling studies show that the increase in the atmospheric burden of O₃ is a combination of a strong O₃ production due to precursors emitted by the fires and an increased destruction of O₃ background levels resulting from reduced peroxy radical concentrations.

[53] While the availability of satellite measurements of tropospheric CO concentrations puts constraints on the CO emissions, uncertainties remain in how to constrain the emissions of NO_x and VOCs resulting in uncertainties in the estimated O₃ production. Another unknown is the emissions injection height of the fires.

[54] The results of this study indicate that fires in the boreal region can have a significant impact on the O₃ production over large parts of the Northern Hemisphere. We focused our investigations on the wildfires in Canada and Alaska from summer 2004, that have been a record for this region, but comparable or even larger impacts might occur from fires in Siberia. With climate change and the possibility of increased fire activity in the Northern latitudes as a result of more frequent and/or more severe droughts and increased direct human impact [Mollicone et al., 2006], O₃ production from boreal fires might gain in importance in the future.

[55] **Acknowledgments.** The authors greatly appreciate the helpful comments provided by Brian Ridley and John Orlando and the two anonymous reviewers. We acknowledge Greg Frost and Stu McKeen for providing the EPA emission inventory. Measurements at PICO-NARE are funded by NOAA Office of Global Programs grants NA16GP1658, NA86GP0325, NA03OAR4310002, and NSF grants ATM0215843 and INT-0110397. The work was supported by NASA grants EOS/03-0601-0145 and NNG04GA459. NCAR is operated by the University Corporation of Atmospheric Research under sponsorship of the National Science Foundation.

References

- Andreae, M. O., and P. Merlet (2001), Emissions from trace gases and aerosols from biomass burning, *Global Biogeochem. Cycles*, *15*, 955–966.
- Andreae, M. O., B. E. Anderson, D. R. Blake, J. D. Bradshaw, J. E. Collins, G. L. Gregory, G. W. Sachse, and M. C. Shipham (1994), Influence of plumes from biomass burning on atmospheric chemistry over the equatorial and tropical South Atlantic during CITE 3, *J. Geophys. Res.*, *99*, 12,793–12,808.
- Averill, C., D. Mazzone, J. Logan, L. Tong, D. Diner, and Q. Li (2005), Combining MISR and MODIS data to automatically catalog smoke plumes in North America, *Earth Obs.*, *17*(6), 11–12.
- Bertschi, I. T., and D. A. Jaffe (2005), Long-Range Transport of ozone, carbon monoxide, and aerosols to the NE Pacific troposphere during the summer of 2003: Observations of smoke plumes from Asian boreal fires, *J. Geophys. Res.*, *110*, D05303, doi:10.1029/2004JD005135.
- Browell, E. V., et al. (2003), Large scale ozone and aerosol distributions, air mass characteristics, and ozone fluxes over the western pacific ocean in late winter/early spring, *J. Geophys. Res.*, *108*(D20), 8805, doi:10.1029/2002JD003290.
- Chameides, W. L., and A. Tan (1981), The two dimensional diagnostic model for tropospheric OH: An uncertainty analysis, *J. Geophys. Res.*, *86*, 5209–5223.
- Damoah, R., N. Spichtinger, R. Servranckx, M. Fromm, E. W. Eloranta, I. A. Razenkov, P. James, M. Shulski, C. Forster, and A. Stohl (2006), Transport modeling of a pyro-convective event in Alaska 2005, *Atmos. Chem. Phys.*, *6*, 173–185.
- Draper, N. R., and H. Smith (1998), *Applied Regression Analysis*, John Wiley, Hoboken, N. J.
- Forster, C., et al. (2001), Transport of boreal forest fire emissions from Canada to Europe, *J. Geophys. Res.*, *106*, 22,887–22,906.
- Fromm, M., R. Bevilacqua, R. Servranckx, J. Rosen, J. P. Thayer, J. Herman, and D. Larko (2005), Pyro-cumulonimbus injection of smoke to the stratosphere: Observations and impact of a super blowup in northwestern Canada on 3–4 August 1998, *J. Geophys. Res.*, *110*, D08205, doi:10.1029/2004JD005350.
- Gerbig, C. D., et al. (1996), Fast response resonance fluorescence CO measurements aboard the C130: Instrument characterization and measurements made during North Atlantic Regional Experiment 1993, *J. Geophys. Res.*, *101*, 29,229–29,238.
- Gerbig, C. D., S. Schmitgen, D. Kley, A. Volz-Thomas, K. Dewey, and D. Haaks (1999), An improved fast-response vacuum-UV resonance fluorescence CO instrument, *J. Geophys. Res.*, *104*, 1699–1704.
- Goode, J. G., R. J. Yokelson, D. E. Ward, R. A. Susott, R. E. Babbitt, M. A. Davies, and W. M. Hao (2000), Measurements of excess O₃, CO₂, CO, CH₄, C₂H₄, C₂H₂, HCN, NO, NH₃, HCOOOH, CH₃COOH, HCHO, and CH₃OH in 1997 Alaskan biomass burning plumes by airborne Fourier transform spectroscopy (AFTIR), *J. Geophys. Res.*, *105*, 22,147–22,166.
- Granier, C., et al. (2005), Present and future surface emissions of atmospheric compounds, *Eur. Comm. Rep. EVK 2199900011*, Eur. Union,

- Brussels. (Available at <http://www.aero.jussieu.fr/projet/ACCENT/POET.php>)
- Holloway, J. S., R. O. Jakoubec, D. D. Parrish, C. Gerbig, A. Volz-Thomas, S. Schmitgen, A. Fried, B. Wert, B. Henry, and J. R. Drummond (2000), Airborne intercomparison of vacuum ultraviolet fluorescence and tunable laser diode absorption measurements of tropospheric carbon monoxide, *J. Geophys. Res.*, *105*, 24,251–24,261.
- Honrath, R. E., R. C. Owen, M. Val Martin, J. S. Reid, K. Lapina, P. Fialho, M. P. Dziobak, J. Kleissl, and D. L. Westphal (2004), Regional and hemispheric impacts of anthropogenic and biomass burning emissions on summertime CO and O₃ in the North Atlantic lower free troposphere, *J. Geophys. Res.*, *109*, D24310, doi:10.1029/2004JD005147.
- Horowitz, L. W., et al. (2003), A global simulation of tropospheric ozone and related tracers: Description and evaluation of MOZART, version 2, *J. Geophys. Res.*, *108*(D24), 4784, doi:10.1029/2002JD002853.
- Jacob, D. J., et al. (1992), Summertime photochemistry of the troposphere at high northern latitudes, *J. Geophys. Res.*, *97*, 16,421–16,431.
- Jaffe, D., I. Bertsch, L. Jaegle, P. Novelli, J. S. Reid, H. Tanimoto, R. Vingarzan, and D. L. Westphal (2004), Long-range transport of Siberian biomass burning emissions and impact on surface ozone in western North America, *Geophys. Res. Lett.*, *31*, L16106, doi:10.1029/2004GL020093.
- Kistler, R., et al. (2001), The NCEP-NCAR 50-year reanalysis: Monthly means CD-ROM and documentation, *Bull. Am. Meteorol. Soc.*, *82*, 247–268.
- Kleissl, J., R. E. Honrath, H. P. Dziobak, D. M. Tanner, M. V. Martin, R. C. Owen, and D. Helmig (2007), Occurrence of upslope flows at the Pico mountaintop observatory: A case study of orographic flows on a small, volcanic island, *J. Geophys. Res.*, doi:10.1029/2006JD007565, in press.
- Lamarque, J.-F., P. Hess, L. Emmons, L. Buja, W. Washington, and C. Granier (2005), Tropospheric ozone evolution between 1890 and 1990, *J. Geophys. Res.*, *110*, D08304, doi:10.1029/2004JD005537.
- Lapina, K., R. E. Honrath, R. C. Owen, M. Val Martin, and G. Pfister (2006), Evidence of significant large-scale impacts of boreal fires on ozone levels in the midlatitude Northern Hemisphere free troposphere, *Geophys. Res. Lett.*, *33*, L10815, doi:10.1029/2006GL025878.
- Levy, H., II, J. D. Mahlman, and W. J. Moxim (1985), Tropospheric ozone: The role of transport, *J. Geophys. Res.*, *90*, 3753–3772.
- Marengo, A., et al. (1998), Measurement of ozone and water vapour by Airbus in-service aircraft: The MOZIC airborne program, an overview, *J. Geophys. Res.*, *103*, 25,631–25,642.
- Mauzerall, D. L., D. J. Jacob, S.-M. Fan, J. D. Bradshaw, G. L. Gregory, G. W. Sachse, and D. R. Blake (1996), Origin of tropospheric ozone at remote high northern latitudes in summer, *J. Geophys. Res.*, *101*, 4175–4188.
- Mauzerall, D. L., J. A. Logan, D. J. Jacob, B. E. Anderson, D. R. Blake, J. D. Bradshaw, B. Heikes, G. W. Sachse, H. Singh, and B. Talbot (1998), Photochemistry in biomass burning plumes and implications for tropospheric ozone over the tropical South Atlantic, *J. Geophys. Res.*, *103*, 8401–8423.
- McKeen, S. A., G. Wotawa, D. D. Parrish, J. S. Holloway, M. P. Buhr, G. Hübler, F. C. Fehsenfeld, and J. F. Meagher (2002), Ozone production from Canadian wildfires during June and July of 1995, *J. Geophys. Res.*, *107*(D14), 4192, doi:10.1029/2001JD000697.
- Mollicone, D., H. D. Eva, and F. Achard (2006), Human role in Russian wildfires, *Nature*, *440*, 436–437.
- Nedelec, P., J. P. Cammas, V. Thouret, G. Athier, J. M. Cousin, C. Legrand, C. Abonnel, F. Lecoq, G. Cayez, and M. Marizy (2003), An improved infra-red carbon monoxide analyser for routine measurements aboard commercial Airbus aircraft: Technical validation and first scientific results of the MOZIC program, *Atmos. Chem. Phys.*, *3*, 1551–1564.
- Owen, R. C., O. R. Cooper, A. Stohl, and R. E. Honrath (2006), An analysis of the mechanisms of North American pollutant transport to the central North Atlantic lower free troposphere, *J. Geophys. Res.*, *111*, D23S58, doi:10.1029/2006JD007062.
- Parrish, D. D., J. S. Holloway, M. Trainer, P. C. Murphy, G. L. Forbes, and F. C. Fehsenfeld (1993), Export of North American ozone pollution to the North Atlantic Ocean, *Science*, *259*, 1436–1439.
- Parrish, D. D., J. S. Holloway, and F. C. Fehsenfeld (1994), Routine, continuous, measurement of carbon monoxide with parts per billion precision, *Environ. Sci. Technol.*, *28*, 1615–1618.
- Pfister, G., P. G. Hess, L. K. Emmons, J.-F. Lamarque, C. Wiedinmyer, D. P. Edwards, G. Pétron, J. C. Gille, and G. W. Sachse (2005), Quantifying CO emissions from the 2004 Alaskan wildfires using MOPITT CO data, *Geophys. Res. Lett.*, *32*, L11809, doi:10.1029/2005GL022995.
- Ramaswamy, V., et al. (2001), Radiative forcing of climate change, in *Climate Change 2001: The Scientific Basis*, edited by J. T. Houghton et al., pp. 349–416, Cambridge Univ. Press, New York.
- Ryerson, T. B., et al. (1998), Emissions lifetimes and ozone formation in power plant plumes, *J. Geophys. Res.*, *103*, 22,569–22,584.
- Sachse, G. W., G. F. Hill, L. O. Wade, and M. G. Perry (1987), Fast-response, high precision carbon monoxide sensor using a tunable diode laser absorption technique, *J. Geophys. Res.*, *92*, 2071–2081.
- Schlager, H., et al. (1997), In situ observations of air traffic emission signatures in the North Atlantic flight corridor, *J. Geophys. Res.*, *102*, 10,739–10,750.
- Tie, X., G. Brasseur, L. Emmons, L. Horowitz, and D. Kinnison (2001), Effects of aerosols on tropospheric oxidants: A global model study, *J. Geophys. Res.*, *106*, 2931–2964.
- Tie, X., S. Madronich, S. Walters, D. P. Edwards, P. Ginoux, N. Mahowald, R. Zhang, C. Luo, and G. Brasseur (2005), Assessment of the global impact of aerosols on tropospheric oxidants, *J. Geophys. Res.*, *110*, D03204, doi:10.1029/2004JD005359.
- Val Martin, M., R. E. Honrath, R. C. Owen, G. Pfister, P. Fialho, and F. Bartsa (2006), Significant enhancements of nitrogen oxides, black carbon and ozone in the North Atlantic lower free troposphere resulting from North American boreal wildfires, *J. Geophys. Res.*, doi:10.1029/2006JD007530, in press.
- Wofsy, S. C., et al. (1992), Atmospheric chemistry in the arctic and sub-arctic: Influence of natural fires, industrial emissions, and stratospheric inputs, *J. Geophys. Res.*, *97*, 16,731–16,746.
- Wotawa, G., and M. Trainer (2000), The influence of Canadian forest fires on pollutant concentrations in the United States, *Science*, *288*, 324–328.
- Yokelson, R. J., I. T. Bertsch, T. J. Christian, P. V. Hobbs, D. E. Ward, and W. M. Hao (2003), Trace gas measurements in nascent, aged, and cloud-processed smoke from African savanna fires by airborne Fourier transform infrared spectroscopy (AFTIR), *J. Geophys. Res.*, *108*(D13), 8478, doi:10.1029/2002JD002322.

M. A. Avery and G. W. Sachse, NASA Langley Research Center, M.S. 483, Hampton, VA 23681, USA. (m.a.avery@larc.nasa.gov; g.w.sachse@larc.nasa.gov)

E. V. Browell, NASA Langley Research Center, M.S. 401A, Hampton, VA 23681-0001, USA. (edward.v.browell@nasa.gov)

L. K. Emmons, P. G. Hess, J.-F. Lamarque, and G. G. Pfister, National Center for Atmospheric Research, 3350 Mitchell Lane, Boulder, CO 80302, USA. (emmons@ucar.edu; hess@ucar.edu; lamar@ucar.edu; pfister@ucar.edu)

J. S. Holloway and T. B. Ryerson, NOAA Aeronomy Laboratory, M.S. R/AL7, 325 Broadway, Boulder, CO 80305, USA. (thomas.b.ryerson@noaa.gov)

R. Honrath, R. C. Owen, and M. Val Martin, Michigan Technological University, 1400 Townsend Drive, Houghton, MI 49931-1295, USA. (reh@mtu.edu; rcowen@mtu.edu; mvalmart@mtu.edu)

P. Nedelec, CNRS Laboratoire d'Aerologie, 14 Avenue E. Belin, 31400 Toulouse, France. (nedp@aero.obs-mip.fr)

R. Purvis, Facility for Airborne Atmospheric Measurement (FAAM), Building 125, Cranfield University, Cranfield MK43 0AL, UK. (rupu@faam.ac.uk)

H. Schlager, Institute of Atmospheric Physics, German Aerospace Center (DLR) Oberpfaffenhofen, 82234 Wessling, Germany. (hans.schlager@dlr.de)